

# Whispering gallery mode lasing from hexagonal shaped layered lead iodide crystals

Liu, Xinfeng; Ha, Son Tung; Zhang, Qing; de la Mata, Maria; Magen, César; Arbiol, Jordi; Sum, Tze Chien; Xiong, Qihua

2015

Liu, X., Ha, S. T., Zhang, Q., de la Mata, M., Magen, C., Arbiol, J., et al. (2015). Whispering gallery mode lasing from hexagonal shaped layered lead iodide crystals. *ACS nano*, 9(1), 687-695.

<https://hdl.handle.net/10356/79463>

<https://doi.org/10.1021/nn5061207>

---

© 2015 American Chemical Society. This is the author created version of a work that has been peer reviewed and accepted for publication by ACS Nano, American Chemical Society. It incorporates referee's comments but changes resulting from the publishing process, such as copyediting, structural formatting, may not be reflected in this document. The published version is available at: [<http://dx.doi.org/10.1021/nn5061207>].

*Downloaded on 09 Apr 2024 17:53:56 SGT*

# Whispering Gallery Mode Lasing from Hexagonal Shaped Layered Lead Iodide Crystals

*Xinfeng Liu,<sup>1,2,#</sup> Son Tung Ha,<sup>1,#</sup> Qing Zhang,<sup>1</sup> Maria de la Mata,<sup>3</sup> Jordi Arbiol,<sup>3,4</sup> Tze Chien Sum<sup>1,2,5,\*</sup> Qihua Xiong,<sup>1,2,6,\*</sup>*

<sup>1</sup>Division of Physics and Applied Physics, School of Physical and Mathematical Sciences, Nanyang Technological University, Singapore 637371

<sup>2</sup>Energy Research Institute @ NTU (ERI@N), Nanyang Technological University, 50 Nanyang Drive, Singapore 637553

<sup>3</sup>Institut de Ciència de Materials de Barcelona, ICMAB-CSIC, E-08193 Bellaterra, CAT, Spain

<sup>4</sup>Institució Catalana de Recerca i Estudis Avançats (ICREA), 08010 Barcelona, CAT, Spain

<sup>5</sup>Singapore-Berkeley Research Initiative for Sustainable Energy, 1 Create Way, Singapore 138602

<sup>6</sup>NOVITAS, Nanoelectronics Centre of Excellence, School of Electrical and Electronic Engineering, Nanyang Technological University, Singapore, 639798

<sup>#</sup> These authors contribute equally to this work.

Correspondences should be addressed, Email: [Tzechien@ntu.edu.sg](mailto:Tzechien@ntu.edu.sg) and [Qihua@ntu.edu.sg](mailto:Qihua@ntu.edu.sg).

## **ABSTRACT**

We report on the synthesis and optical gain properties of regularly shaped lead iodide ( $\text{PbI}_2$ ) platelets with thickness ranging from 10 to 500 nm using chemical vapor deposition (CVD). The as-prepared single crystalline platelets exhibit a near band edge emission of  $\sim 500$  nm. Whispering gallery mode (WGM) lasing from individual hexagonal shaped  $\text{PbI}_2$  platelets is demonstrated in the temperature range from 77 to 210 K – where the lasing modes are supported by platelets as thin as 45 nm. The FDTD simulation and the edge-length dependent threshold confirm the planar WGM lasing mechanism in such hexagonal shaped  $\text{PbI}_2$  platelet. Through a comprehensive study of power-dependent photoluminescence (PL) and time-resolved PL spectroscopy, we ascribe the WGM lasing to be biexcitonic in nature. Moreover, for different thickness of platelet, the lowest lasing threshold occurs in platelets of  $\sim 120$  nm, attributing to the formation of a good Fabry-Pérot resonance cavity in the vertical direction between the top and bottom platelet surfaces that enhance the reflection. Our present study demonstrates the feasibility of planar light sources based on layered semiconductor materials and their thickness dependent threshold characteristic is beneficial for the optimization of layered material based optoelectronic devices.

**KEYWORDS:** Whispering gallery mode (WGM), lasing, layered materials, lead iodide, hexagonal platelet, Fabry-Pérot cavity

## INTRODUCTION

Lead iodide ( $\text{PbI}_2$ ), which consists of a repeating unit of a hexagonally closed-packed layer of lead ions sandwiched between two layers of iodide ions (layered material), has some unique optical and electronic properties, which is quite different from traditional semiconductor gain material such as,  $\text{CdS}$ ,  $\text{ZnO}$  and  $\text{GaN}$  *et al.*<sup>1-5</sup> In these layered semiconductor materials ( $\text{PbI}_2$ ,  $\text{BiI}_3$ ,  $\text{HgI}_2$ ,  $\text{Bi}_2\text{S}_3$ , and  $\text{Sb}_2\text{S}_3$ ), spatial confinement of charge carriers in multilayered or multi-quantum-well structures has many potential utilities in photovoltaic, detectors, sensors and photo catalysis.<sup>1, 6, 7</sup> Additionally, this kind of layered material would provide us with an ideal system to investigate the fundamental properties of excitons in a highly ionic environment and low dimensionality, where the exciton-phonon coupling is expected to be unprecedented compared with conventional semiconductors.<sup>3, 4</sup>

On the other hand,  $\text{PbI}_2$  has been extensively employed as a stable nuclear radiation detector.<sup>8-10</sup> It converts the X-ray or  $\gamma$ -ray photons directly to electric charges (current carriers) that are stored in a capacitor in each pixel that improves the quality of the image compared with the traditional phosphorous layer. Working as a scintillation detector, many electron-hole pairs are firstly generated and thermalized in the conduction and valence band after the absorption of the X-ray or  $\gamma$ -ray. Then electron and holes migrate through the material, trapping at defects may occur, energy losses are probable due to non-radiative recombination. Therefore, understanding the behavior of electron and hole under strong light excitation is beneficial to the design of the photo-detector under relatively strong X or  $\gamma$ -ray exposure intensities.

Moreover,  $\text{PbI}_2$  is one of the precursors to synthesize lead halide perovskites, which have shown tremendous advances in photovoltaics for the past few years, and have also been demonstrated as a promising optical gain material for amplified spontaneous emission (ASE) or lasing.<sup>11-13</sup> Deep investigations of the lead halides precursor (e.g., lead iodide) are important towards the understanding of the photo-physics of the inorganic-organic perovskites and their applications in emergent devices.<sup>14, 15</sup> From previous literature, the optical and excitonic properties of single crystalline  $\text{PbI}_2$  films and thin layers have been previously investigated by steady-state and ultrafast spectroscopy techniques.<sup>7, 16-20</sup> As for their synthesis, several special experimental methods have been developed involving sol-gel method,<sup>20</sup> vapor deposition method,<sup>21</sup> and Bridgman's method for growth of  $\text{PbI}_2$  single crystals.<sup>5, 22</sup> However, challenges pertaining to the synthesis of regular-shaped single crystalline  $\text{PbI}_2$  crystals with sub-wavelength thickness, ideal for on-chip optical amplifier and lasers integration with planar optoelectronic devices, remain daunting. Despite of a few researches on linear optical properties, the studies focusing on the recombination and amplification of photon emission in layered  $\text{PbI}_2$  platelets under strong optical excitation are still limited.<sup>23, 24</sup>

In this work, we have synthesized regular-shaped  $\text{PbI}_2$  platelet with thickness ranging from 10 to 500 nm using chemical vapor deposition (CVD) method. The as-prepared single crystalline platelets exhibit a near band-gap emission  $\sim 500$  nm at 77 K. Whispering gallery mode (WGM) lasing from  $\text{PbI}_2$  is demonstrated from individual platelet at temperatures from 77 to 210 K. Lasing modes are supported in

PbI<sub>2</sub> platelets as thin as 45 nm, which is the thinnest planar laser ever reported. Through a comprehensive power-dependent photoluminescence (PL) and time-resolved photoluminescence (TRPL) study, we establish unambiguously that the lasing mechanism originates from biexcitonic recombination. Thickness-dependent lasing measurements reveal that the lowest lasing threshold occurs when the platelet thickness is ~120 nm. We attribute this thickness dependent behavior of lasing threshold to the reflection between the top and bottom surfaces of PbI<sub>2</sub> that forming the Fabry-Pérot resonance cavity in the vertical direction. Our experiment results demonstrate the feasibility of planar light sources based on layered semiconductor materials.

## RESULTS AND DISCUSSION

The synthesis procedure of PbI<sub>2</sub> single crystals can be found in the methods part. The as-grown PbI<sub>2</sub> platelets exhibit well-defined triangular or hexagonal structures with thickness ranging from 10 to 500 nm and the edge lengths from several to tens of micrometers (hexagonal shaped PbI<sub>2</sub> platelet was our main focus in this work). Figure 1a-d exhibits the optical images of four typical shaped as-grown PbI<sub>2</sub> platelets. Their thicknesses are around 40, 70, 105 and 500 nm, respectively, which is determined by the atomic force microscopy (AFM) data (supporting information Figure S1). The average surface roughness of these PbI<sub>2</sub> platelets is ~2 nm, which is perfectly flat on an optical level. The flat surface is an essential criterion to achieve a high quality optical cavity. X-ray diffraction pattern shown in Figure S2 suggests the 2H hexagonal crystalline structure. Raman spectroscopy characterization of the

as-prepared sample in Figure S3 also suggests the forming of PbI<sub>2</sub> crystals. More detailed characterization was also carried out using transmission electron microscopy (TEM) and a scanning TEM (STEM) to assess the structure, crystallinity and elemental composition of the as grown PbI<sub>2</sub> sample. Figure 1e is a typical TEM image of the PbI<sub>2</sub> platelet; Figure 1f and g give the corresponding Pb and I mapping images obtained by energy dispersive x-ray spectroscopy. They confirm the elemental uniformity of the as-grown PbI<sub>2</sub> platelet over the whole platelet. The high resolution cross-sectional TEM image (see Figure 1h) of the platelet shows that the interlayer space is around 0.703 nm, which is in good agreement with the (0001) plane spacing theoretical value.<sup>25, 26</sup> The atomic structures of the layer atoms in planar view are also studied by high resolution TEM (HRTEM). Figure 1i is the HRTEM image of the layer PbI<sub>2</sub>, where the middle inset overlapping the structure corresponds to the simulated HRTEM image. Notice that red and blue dashed circles represent the positions of top/lower-layer of iodine atoms, which are indistinguishable from the HRTEM images, according to the image simulations performed. In the center position encircled by these iodine atoms is the Pb atom, which is relatively brighter compared to the iodine atoms, also in good agreement with our HRTEM image simulations. Figure 1i bottom inset shows the corresponding Fast Fourier Transform (FFT) pattern of the HRTEM image showing the six-fold symmetric diffraction spot, which is consistent with our XRD results. All these characterizations attest the high crystallinity of these as-synthesized PbI<sub>2</sub> platelets, which is an important factor for achieving photon amplification in these naturally-formed whispering gallery cavities.

An individual PbI<sub>2</sub> platelet was optically pumped using 400 nm wavelength femtosecond laser pulses at 77 K. The optical pump configuration is schematically shown in Figure 2a. The pump laser was focused to a spot size of  $\sim 40\ \mu\text{m}$  using a 20 $\times$  objective. Figure 2b shows the power-dependent emission spectra of a typical PbI<sub>2</sub> hexagonal platelet (thickness  $\sim 150\ \text{nm}$ ; edge length  $\sim 13\ \mu\text{m}$ ). A broad spontaneous emission band centered at 500 nm with a full width at half maximum (FWHM) of  $\lambda_{\text{FWHM}} \sim 6\ \text{nm}$  can be observed under relatively lower pump fluence excitation (*e.g.*,  $P < 100\ \mu\text{J}/\text{cm}^2$ ). With increasing the pump fluence ( $\sim 200\ \mu\text{J}/\text{cm}^2$ ), a relatively sharp peak centered at around 502 nm with a  $\lambda_{\text{FWHM}}$  of  $\sim 3.5\ \text{nm}$  appears at the longer wavelength side of the main spontaneous emission peak. When the pump fluence is further increased ( $P > 200\ \mu\text{J}/\text{cm}^2$ ), the emission peak intensity increases sharply and the FWHM of the emission peak reduces to  $\sim 1.4\ \text{nm}$  – exhibiting lasing action.<sup>27, 28</sup> Figure 2b inset shows the peak emission intensity as a function of excitation intensity (light input – light output, or ‘ $L - L$  curve’ – right axis) and the FWHM of the platelet emission (left axis). At the lasing threshold  $P_{\text{th}} \sim 200\ \mu\text{J}/\text{cm}^2$ , we observed a clear change in gradient in the  $L - L$  curve with a concurrent sharp decrease in FWHM. Beyond the threshold, the lasing peak intensity increases linearly with excitation fluence. It should be noted that only one peak is observed in the micrometer cavity, which is probably the results of broadening of lasing modes due to these different modes share almost the same threshold at low temperature range. Time-resolved PL study is employed (see Figure 2c-d) to further validate the occurrence of the lasing action. Below the threshold, an Auger-limited spontaneous emission lifetime of  $\sim 70$



ps is obtained. Above the threshold, the PL dynamics at the emission peak shows a dominant ultrafast decay channel with a lifetime of  $\sim 10$  ps (limited by the system response of the streak camera over the time window) and a small spontaneous emission component with a lifetime of  $\sim 70$  ps.

To prove that whispering gallery mode (WGM) lasing occurs in the hexagonal shaped  $\text{PbI}_2$  platelet, optical mode simulations are performed to study the field distribution in the resonant cavity modes. Optical simulations are performed using commercial finite-difference time-domain (FDTD) simulation software (Lumerical) to study the mode distribution in  $\text{PbI}_2$  platelet grown on mica substrate. To simplify the system from 3D to 2D, we introduce the effective index of refraction – mainly the planar waveguide model. Then we simulate the mode distribution in 2D system using the effective index rather than the index of the material. In Figure 3a shows an optical image of a representative hexagonal  $\text{PbI}_2$  platelet with thickness  $\sim 150$  nm and edge length  $\sim 13$   $\mu\text{m}$ , respectively. The PL emission image (the excitation laser was filtered out by a long pass filter) of the same hexagonal  $\text{PbI}_2$  platelet above the lasing threshold can be clearly seen in Figure 3b. The bright spots at the hexagonal corners indicate the out coupling of the laser pulses at these locations. It suggests that a good mode confinement in the platelet plane is obtained, leading to an in-plane emission. Figure 3c-d shows the simulation results on the absolute electric field distribution inside the hexagonal platelet (thickness  $\sim 150$  nm; edge length  $\sim 13$   $\mu\text{m}$ ) when the transverse magnetic (TM, effective index  $\sim 2.18$ ) and transverse electric (TE, effective index  $\sim 1.97$ ) modes dominate respectively. In these two scenarios, the optical fields

are well confined inside the cavities and reflections between the hexagonal facets/corners results in the formation of the WGMs. However, compared to the TE mode, the TM mode has a larger effective refractive index (the TM and TE modes should be not the same order due to the effective index is generally higher for TE than TM mode of the same order) and relatively strong filed intensity, thus a lower lasing threshold can be expected from the TM mode.<sup>29</sup> This is evident from the similarity between the optical image (see Figure 3b) and TM mode simulations (see Figure 3c). To experimentally prove our simulation result, using confocal microscopy system, we measured the polarization dependent lasing intensities. The measured polarization dependent lasing intensity is exhibited in Figure S4. It can be seen that the lasing intensity shows a maximum when the polarization is along with the 0 degree axis, which suggests that the TM mode dominates the signal (if the TE mode dominates, the maximum signal happens when the polarization angle is in 90 degree direction). Another evidence to confirm the WGM mode lasing rather than Fabry-Pérot lasing in the vertical direction is the  $1/L^2$  relationship between the platelet edge length (L) and the lasing threshold. The related data and discussion will be shown in the later part.

To elucidate the lasing mechanism, pump fluence dependent time-integrated PL of a single  $\text{PbI}_2$  platelet at 77 K is performed and the results are given in Figure 4a. The inset shows a representative PL spectrum (with a pumping fluence  $\sim 40 \mu\text{J}/\text{cm}^2$ ) with two dominant peaks labeled as Peak X and Peak XX which are deconvolved from the Gaussian fitting of the broad emission peak. The intensity of Peak X (centered at 498 nm) is linearly proportional (slope  $\sim 0.95$ ) to the excitation fluence

when it is below  $\sim 90 \mu\text{J}/\text{cm}^2$ , and then increases as the square-root of the excitation fluence above that. On the other hand, Peak XX (centered at 505 nm) exhibits a quadratic dependence with excitation fluence up to  $\sim 20 \mu\text{J}/\text{cm}^2$  and then increases almost linearly proportional (with slope  $\sim 0.9$ ) to the excitation fluence up to  $\sim 200 \mu\text{J}/\text{cm}^2$ . Beyond that, the Peak XX increases superlinearly with pump fluence to yield a lasing action. Such pump fluence dependent emission characteristics of Peak X and XX closely resembles those of exciton and biexciton luminescence reported for Si, GaN/AlN and perovskite materials, respectively.<sup>30-32</sup> Therefore, we attribute the emissions at Peak X and XX to originate from the single exciton and biexciton emission, respectively.<sup>33</sup> Radiative recombination of a biexciton produces a photon ( $\hbar\omega_{\text{XX}}$ ) and an exciton ( $E_{\text{X}}$ ) and hence,  $\hbar\omega_{\text{XX}} = E_{\text{XX}} - E_{\text{X}} = E_{\text{X}} + \Delta_{\text{XX}}$ , where  $E_{\text{XX}}$  is biexciton recombination energy and  $\Delta_{\text{XX}}$  is the biexciton binding energy.<sup>34, 35</sup> The biexciton binding energy,  $\sim 32 \text{ meV}$ , can be deduced from the energy difference between the single exciton  $E_{\text{X}}$  ( $\hbar\omega_{\text{X}}$ ) and bioexciton  $\hbar\omega_{\text{XX}}$ , which agrees with the value of  $\sim 30 \text{ meV}$  reported previously.<sup>36</sup> The PL decay transients of the single excitons (Peak X) and the biexcitons (Peak XX) both exhibit a mono-exponential decay behavior (see Figure 4b) and can be well-fitted with a single recombination lifetime of  $\sim 83 \pm 4 \text{ ps}$  and  $47 \pm 3 \text{ ps}$  for the excitons and biexcitations, respectively.<sup>37, 38</sup> The ratio of biexciton lifetime versus that of the exciton is  $\sim 1.8$ ; which is very close to the intuitive relation of  $\tau_{\text{X}}/\tau_{\text{XX}} = 2$  where a biexciton is treated like a system of two weakly coupled excitons with half the exciton's lifetime.<sup>39, 40</sup>

After validating the lasing mechanism to be biexcitonic in origin, we turn our

attention to the intrinsic lasing properties (*i.e.* wavelength and threshold) as a function of temperature. Figure 4c shows the normalized emission spectra recorded at the above threshold for a single PbI<sub>2</sub> platelet from 77 to 210 K, with the pumping fluence of 0.25, 0.4, 0.7, 1.2 and 2.5 mJ/cm<sup>2</sup>, respectively. When the temperature increases to be higher than 210 K, the lasing action ceases for the PbI<sub>2</sub> platelet. As the lattice temperature varies, the dominant lasing peak redshifts (see Figure 4d) from 496 nm to 510 nm, suggesting a bandgap narrowing.<sup>41, 42</sup> Furthermore, the lasing peak is always located at the longer wavelength side of the broad emission peak. It means that the lasing behavior is always related to the biexciton formation and recombination at this temperature range (77-210 K). The lasing threshold increases from ~200 μJ/cm<sup>2</sup> to ~2.3 mJ/cm<sup>2</sup> when the sample temperature increases from 77 to 210 K (see Figure 4d). This behavior can be fitted by an exponential function (lasing threshold  $\sim \exp^{T/T_0}$ ) describing the thermal broadening of the gain spectrum, and we obtain a characteristic temperature of  $T_0 = 45$  K for the PbI<sub>2</sub> platelet laser (see Figure 4d). This characteristic temperature is the description of the thermal stability of this material, which explains why no lasing can be obtained at room temperature. On the contrary, some conventional semiconductors exhibit higher characteristic temperatures, *e.g.*, 90-130 K for ZnO and 160-246 K for GaN.<sup>43, 44</sup>

As the different platelet size (*i.e.* edge length  $L$ ) affects the mode confinement and hence the lasing threshold,<sup>45</sup> we carefully conducted this study using a series of hexagonal PbI<sub>2</sub> platelets with similar edge lengths (*i.e.*  $20 \pm 2$  μm), while investigating the thickness dependent lasing properties. Figure 5 a-d show the PL

spectra from four typical PbI<sub>2</sub> platelets with different thickness when they are optically pumped by a pulsed laser at 77 K. The thicknesses of PbI<sub>2</sub> in Figure 5 a-d are 40, 120, 200 and 300 nm, respectively. At lower pump fluence, the PL spectra are broad; however, as the pump influence increased above the lasing threshold, a sharp peak at around 500 nm occurs with a FWHM of 1 nm. A plot of the intensity peak versus pump fluence (insets of Figure 5a-d) shows the transition from spontaneous to stimulated emission. The corresponding thresholds for the 40, 120 and 300 nm thick PbI<sub>2</sub> platelets are 442, 54 and 280  $\mu\text{J}/\text{cm}^2$ , respectively. Figure 5e summarizes the PbI<sub>2</sub> lasing threshold with different thickness ranging from 45 nm to 300 nm. It is very interesting that the lowest lasing threshold occurs when the layer thickness is  $\sim 122$  nm. In addition, another local minimum is observed at  $\sim 245$  nm.

To investigate the layer thickness dependence of the lasing threshold, the parametric threshold gain,  $G_{\text{th}}$ , is used here to describe our current system. The expression of  $G_{\text{th}}$  is defined as follows,  $G_{\text{th}} = 2\pi n_g / (\Gamma_E \lambda Q)$ , where  $n_g$ ,  $\lambda$ ,  $\Gamma_E$ , and  $Q$  are group index of the material, resonant wavelength, energy confinement factor and quality factor, respectively.<sup>46</sup> As this expression originates from the general gain and loss balance conditions for the rate equation, it is valid for all types of cavity modes. In the case of PbI<sub>2</sub> platelets, the group index and resonant wavelength can be treated approximately independent on the platelet thickness. Furthermore, the lasing modes of PbI<sub>2</sub> for different thickness have almost the same peak width ( $\sim 1$  nm), indicating comparable  $Q$  factors. Therefore, the energy confinement factor  $\Gamma_E$  should play as the dominant role in our scenario. Due to the large edge length ( $\sim 20$

$\mu\text{m}$ ) of  $\text{PbI}_2$ , the WGM loss in the planar direction can be negligible compared to the loss in the vertical direction owes to sub-wavelength thickness ranging from 40 to 300 nm. However, in the vertical direction, the top and bottom surfaces of the  $\text{PbI}_2$  platelet function as mirrors, forming a Fabry-Pérot (F-P) cavity itself. This naturally formed F-P cavity holds maximum energy confinement when the cavity length ( $D$ ) satisfies the following equation,  $D \times n_{\text{PbI}_2} = m \times \lambda / 2$  (see the figure 5e inset), where  $\lambda$  and  $n_{\text{PbI}_2}$  are resonant wavelength and refractive index, respectively, while  $m$  is an integer.<sup>47, 48</sup> Considering that the lasing wavelength is  $\sim 505$  nm and refractive index of  $\text{PbI}_2$  at 505 nm is  $\sim 2.1$ ,  $\text{PbI}_2$  platelets with thickness of  $\sim 120$  nm and  $\sim 240$  nm would possess the maximum energy confinement ( $\Gamma_E$ ) for thickness in the range from 45 to 300 nm range, then leading to the lowest threshold at these two thickness. This is in good agreement with our experimental observations of the two lowest threshold pump fluences at 122 nm and 245 nm (see Figure 5e). Furthermore, another prove is the biexciton lifetime measurement (with the same excitation power of  $\sim 40 \mu\text{J}/\text{cm}^2$ ) for the  $\text{PbI}_2$  platelets of varying thicknesses, as shown in Figure 5f. It is interesting to note that the 120 nm thick  $\text{PbI}_2$  platelet exhibits the longest biexciton lifetime. Intuitively, this agrees well with the occurrence of the lowest pump threshold as the longer lived biexciton population would facilitate the population inversion and the build-up of lasing in photonic mode lasing conditions. Moreover, the maximum PL intensity for 120 nm thick  $\text{PbI}_2$  platelet (see Figure S5) further supports our argument. Therefore, we can conclude that the lasing behavior in hexagonal  $\text{PbI}_2$  structure is predominately determined by the planar WGM modes, and also partially affected by

the thickness of the platelet.

Lastly, a plot of hexagonal PbI<sub>2</sub> platelet edge length ( $L$ ) versus lasing threshold is shown in Figure 6. To minimize the effect of different thickness, a series of PbI<sub>2</sub> platelets with comparable thickness ( $\sim 200$  nm) but different edge lengths (from 14 to 40  $\mu\text{m}$ ) are selected for this study (see inset in Figure 6). The best-fit line (red curve) is approximately  $1/L^2$ , which indicates the lasing threshold is dominantly dependent on the parameter of PbI<sub>2</sub> platelet edge length. Previous studies have shown that both WGM quality factor ( $Q$ ) and confinement factor ( $\Gamma$ ) depend critically on disk diameter.<sup>46, 49, 50</sup> Since lasing threshold is inversely proportional to  $Q$  and  $\Gamma$ , a  $1/L^2$  relationship is expected for platelet edge length and lasing threshold. Considering the thickness-dependent threshold discussion, we know that the lasing threshold scales inversely with the power of platelet edge length, rather than with platelet thickness. This provides clear evidence of WGM lasing rather than Fabry-Pérot lasing in the vertical direction. This conclusion is consistent with our previous simulation results as shown in Figure 3c.

## CONCLUSIONS

In summary, we have demonstrated WGM lasing in single crystalline hexagonal PbI<sub>2</sub> platelet fabricated using CVD method. Through power-dependent PL and TRPL studies, we establish that the lasing mechanism originates from biexciton recombination. Platelet thickness dependent lasing measurements reveal that the lowest threshold of lasing occurs when the thickness of the platelet is  $\sim 120$  nm for a series of PbI<sub>2</sub> platelets with comparable edge length. This thickness dependent

behavior of threshold can be well explained by the reflection enhancement in the Fabry-Pérot resonance cavity in the vertical direction as validated by the lifetime measurements. Our results demonstrate the feasibility of planar coherent light sources based on layered semiconductor materials, and the thickness-dependent threshold study is of vital importance for the optimization of layered material based optoelectronic devices.



## **METHODS**

### **PbI<sub>2</sub> Synthesis process**

Lead iodide powder (Aldrich, 99.999%) was the reaction source and placed into a quartz tube which is mounted on a single zone furnace (Lindberg/Blue M TF55035C-1). Fresh cleaved muscovite mica substrate (1×3 cm<sup>2</sup>) was cleaned by acetone and then placed in the downstream region inside the quartz tube. The quartz tube was evacuated to a base pressure of 2 mTorr, and then followed by a 30 sccm flow of high purity Ar premixed with 5% H<sub>2</sub> gas. The temperature and pressure inside the quartz tube were set and stabilized to desired values for each halide (380 °C & 200 torr). The synthesis process was finished within 20 minutes and then the furnace cool down to room temperature naturally.

### **Steady-state and Time-resolved Photoluminescence Spectroscopy**

The excitation pulses (wavelength, 400 nm) are double frequencies from the Coherent Libra<sup>TM</sup> regenerative amplifier (50 fs, 1 KHz, 800 nm) which is seeded by a Coherent Vitesse<sup>TM</sup> oscillator. The pump laser is focused onto samples by a 20× objective. The laser spot is ~40 μm in diameter after objective. For lasing images of the sample, the PL emission signals are imaged on a CCD camera using a long-pass filter to block the laser line. For spectrum measurement, the emission signals from an area (~5 μm × 5 μm) pass through an aperture and are analyzed by a spectrometer equipped with a TE-cooled CCD. For TRPL measurement, the PL emission was collected and dispersed by a 25 cm spectrometer using a 150 g/mm grating. The signal was resolved using an Optronis Streak Camera system (Optoscope<sup>TM</sup>), which has an ultimate temporal resolution of ~10 ps.

### **Numerical simulation**

Cavity simulations are performed using commercial finite-difference time-domain (FDTD) simulation software (Lumerical) to study the optical feedback mechanism allowing laser oscillation in PbI<sub>2</sub> platelet grown on mica substrate.<sup>51</sup> To simplify the

system from 3D to 2D, we introduce the effective index of refraction-mainly the planar waveguide model. Then we simulate the mode distribution in 2D system using the effective index rather than the index of the material. The refractive index of mica and  $\text{PbI}_2$  can be obtained from literatures.<sup>17, 52</sup>

### **Acknowledgements**

Q.X. acknowledges the support from the Singapore National Research Foundation through a NRF fellowship grant (NRF-RF2009-06) and a Competitive Research Program grant (NRF-CRP-6-2010-2), Ministry of Education AcRF Tier 2 Grants (MOE2011-T2-2-051 and MOE2013-T2-1-049), and start-up grant support (M58113004) from Nanyang Technological University (NTU). T.C.S. acknowledges the support from the following research grants: NTU start-up grant (M4080514); SPMS collaborative Research Award (M4080536); and the Ministry of Education (MOE) Academic Research Fund (AcRF) Tier 2 grant MOE2013-T2-1-081. X.F.L. and T.C.S. also acknowledge the financial support by the Singapore National Research Foundation through the Competitive Research Programme under Project No. NRF-CRP5-2009-04 and the Singapore-Berkeley Research Initiative for Sustainable Energy (SinBerRISE) CREATE Programme. J.A. acknowledges the funding from Generalitat de Catalunya 2014 SGR 1638. MdIM thanks CSIC Jae-Predoc program.

### **Supporting information**

Supporting information for the experimental results can be found in the supporting information section. These materials are available free of charge via the Internet at <http://pubs.acs.org>.

## REFERENCES:

1. Sengupta, A.; Jiang, B.; Mandal, K. C.; Zhang, J. Z. Ultrafast Electronic Relaxation Dynamics in PbI<sub>2</sub> Semiconductor Colloidal Nanoparticles: A Femtosecond Transient Absorption Study. *The Journal of Physical Chemistry B* **1999**, 103, 3128-3137.
2. Makino, T.; Watanabe, M.; Hayashi, T.; Ashida, M. Time-resolved luminescence of exciton polaritons in PbI<sub>2</sub>. *Physical Review B* **1998**, 57, 3714-3717.
3. Watanabe, M.; Hayashi, T. Polariton Relaxation and Bound Exciton Formation in PbI<sub>2</sub> Studied by Excitation Spectra. *Journal of the Physical Society of Japan* **1994**, 63, 785-794.
4. Dorner, B.; Ghosh, R. E.; Harbeke, G. Phonon Dispersion in the Layered Compound PbI<sub>2</sub>. *physica status solidi (b)* **1976**, 73, 655-659.
5. Ahuja, R.; Arwin, H.; Ferreira da Silva, A.; Persson, C.; Osorio-Guillén, J. M.; Souza de Almeida, J.; Moyses Araujo, C.; Veje, E.; Veissid, N.; An, C. Y., *et al.* Electronic and optical properties of lead iodide. *Journal of Applied Physics* **2002**, 92, 7219-7224.
6. Sandroff, C.; Hwang, D.; Chung, W. Carrier confinement and special crystallite dimensions in layered semiconductor colloids. *Physical Review B* **1986**, 33, 5953-5955.
7. Goto, T.; Tanaka, H. Exciton study in PbI<sub>2</sub> microcrystallites by pump-probe method. *Solid State Commun.* **1994**, 89, 17-21.
8. Street, R. A.; Ready, S. E.; Van Schuylenbergh, K.; Ho, J.; Boyce, J. B.; Nylén, P.; Shah, K.; Melekhov, L.; Hermon, H. Comparison of PbI<sub>2</sub> and HgI<sub>2</sub> for direct detection active matrix x-ray image sensors. *Journal of Applied Physics* **2002**, 91, 3345-3355.
9. Nikl, M. Scintillation detectors for x-rays. *Measurement Science and Technology* **2006**, 17, R37.
10. Yanagida, T.; Fujimoto, Y.; Yoshikawa, A.; Yokota, Y.; Kamada, K.; Pejchal, J.; Chani, V.; Kawaguchi, N.; Fukuda, K.; Uchiyama, K., *et al.* Development and Performance Test of Picosecond Pulse X-ray Excited Streak Camera System for Scintillator Characterization. *Applied Physics Express* **2010**, 3, 056202.
11. Zhang, Q.; Ha, S. T.; Liu, X.; Sum, T. C.; Xiong, Q. Room-Temperature Near-Infrared High-Q Perovskite Whispering-Gallery Planar Nanolasers. *Nano Lett.* **2014**, 14, 5995-6001.
12. Xing, G.; Mathews, N.; Lim, S. S.; Yantara, N.; Liu, X.; Sabba, D.; Grätzel, M.; Mhaisalkar, S.; Sum, T. C. Low-temperature solution-processed wavelength-tunable perovskites for lasing. *Nat Mater* **2014**, 13, 476-480.
13. Grätzel, M. The light and shade of perovskite solar cells. *Nat Mater* **2014**, 13, 838-842.
14. Tan, Z.-K.; Moghaddam, R. S.; Lai, M. L.; Docampo, P.; Higler, R.; Deschler, F.; Price, M.; Sadhanala, A.; Pazos, L. M.; Credgington, D., *et al.* Bright light-emitting diodes based on organometal halide perovskite. *Nat Nano* **2014**, 9, 687-692.
15. Lin, Q.; Armin, A.; Nagiri, R. C. R.; Burn, P. L.; Meredith, P. Electro-optics of perovskite solar cells. *Nat Photon* **2014**, advance online publication.
16. Ahmad, A.; Saq'an, S.; Lahlouh, B.; Hassan, M.; Alsaad, A.; El-Nasser, H. Ellipsometric characterization of PbI<sub>2</sub> thin film on glass. *Physica B-Condensed Matter* **2009**, 404, 1-6.
17. Dugan, A. E.; Henisch, H. K. Dielectric properties and index of refraction of lead iodide single crystals. *Journal of Physics and Chemistry of Solids* **1967**, 28, 971-976.
18. Yamamoto, A.; Nakahara, H.; Yano, S.; Goto, T.; Kasuya, A. Exciton Dynamics in PbI<sub>2</sub> Ultra-Thin Microcrystallites. *physica status solidi (b)* **2001**, 224, 301-305.
19. Ando, M.; Yazaki, M.; Katayama, I.; Ichida, H.; Wakaiki, S.; Kanematsu, Y.; Takeda, J.

Photoluminescence dynamics due to biexcitons and exciton-exciton scattering in the layered-type semiconductor PbI<sub>2</sub>. *Physical Review B* **2012**, 86.

20. Lifshitz, E.; Yassen, M.; Bykov, L.; Dag, I.; Chaim, R. Photodecomposition and Regeneration of PbI<sub>2</sub> Nanometer-Sized Particles, Embedded in Porous Silica Films. *The Journal of Physical Chemistry* **1995**, 99, 1245-1250.

21. Fornaro, L.; Saucedo, E.; Mussio, L.; Gancharov, A. Toward epitaxial lead-iodide films for X-ray digital imaging. *Ieee Transactions on Nuclear Science* **2002**, 49, 2274-2278.

22. Ferreira da Silva, A.; Veissid, N.; An, C. Y.; Pepe, I.; Barros de Oliveira, N.; Batista da Silva, A. V. Optical determination of the direct bandgap energy of lead iodide crystals. *Applied Physics Letters* **1996**, 69, 1930-1932.

23. Brodin, M. S.; Vitrikhovskii, N. I.; Kipen', A. A.; Yamkovaya, L. N.; Yanushevskii, N. I. Influence of crystal size and temperature on the stimulated emission spectrum of CuBr. *Soviet Journal of Quantum Electronics* **1989**, 19, 324.

24. Brodin, M. S.; Blonskiĭ, I. V.; Dobrovol'skiĭ, A. A.; Karataev, V. N.; Kipen', A. A.; Yanushevskii, N. I. Lasing in laminar PbI<sub>2</sub> single crystals. *Soviet Journal of Quantum Electronics* **1986**, 16, 140.

25. Sandroff, C. J.; Kelty, S. P.; Hwang, D. M. Clusters in Solution-Growth and Optical-Properties of Layered Semiconductors with Hexagonal and Honeycombed Structures. *Journal of Chemical Physics* **1986**, 85, 5337-5340.

26. Zheng, Z.; Liu, A. R.; Wang, S. M.; Wang, Y.; Li, Z. S.; Lau, W. M.; Zhang, L. Z. In situ growth of epitaxial lead iodide films composed of hexagonal single crystals. *J. Mater. Chem.* **2005**, 15, 4555-4559.

27. Saxena, D.; Mokkapat, S.; Parkinson, P.; Jiang, N.; Gao, Q.; Tan, H. H.; Jagadish, C. Optically pumped room-temperature GaAs nanowire lasers. *Nature Photonics* **2013**, 7, 963-968.

28. Liu, X.; Zhang, Q.; Xiong, Q.; Sum, T. C. Tailoring the Lasing Modes in Semiconductor Nanowire Cavities Using Intrinsic Self-Absorption. *Nano Lett.* **2013**, 13, 1080-1085.

29. Zhang, Q.; Li, G.; Liu, X.; Qian, F.; Li, Y.; Sum, T. C.; Lieber, C. M.; Xiong, Q. A room temperature low-threshold ultraviolet plasmonic nanolaser. *Nat Commun* **2014**, 5.

30. Kondo, T.; Azuma, T.; Yuasa, T.; Ito, R. Biexciton lasing in the layered perovskite-type material (C<sub>6</sub>H<sub>13</sub>NH<sub>3</sub>)(<sub>2</sub>)PbI<sub>4</sub>. *Solid State Commun.* **1998**, 105, 253-255.

31. Benoit À La Guillaume, C.; Salvan, F.; Voos, M. Investigation of the radiative recombination of the excitonic molecule in Ge and Si. *Journal of Luminescence* **1970**, 1-2, 315-323.

32. Renard, J.; Songmuang, R.; Bougerol, C.; Daudin, B.; Gayral, B. Exciton and Biexciton Luminescence from Single GaN/AlN Quantum Dots in Nanowires. *Nano Lett.* **2008**, 8, 2092-2096.

33. Tanaka, K.; Hosoya, T.; Fukaya, R.; Takeda, J. A new luminescence due to an exciton-exciton collision process in lead iodide induced by two-photon absorption. *Journal of Luminescence* **2007**, 122, 421-423.

34. Klimov, V. I.; Ivanov, S. A.; Nanda, J.; Achermann, M.; Bezel, I.; McGuire, J. A.; Piryatinski, A. Single-exciton optical gain in semiconductor nanocrystals. *Nature* **2007**, 447, 441-446.

35. Park, Y.-S.; Bae, W. K.; Pietryga, J. M.; Klimov, V. I. Auger Recombination of Biexcitons and Negative and Positive Trions in Individual Quantum Dots. *ACS Nano* **2014**, 8, 7288-7296.

36. Frdhlch, D., and Kenkies, R. (1977). *Nuovo Cimento B* 38, 433-438.

37. Liu, X.; Zhang, Q.; Yip, J. N.; Xiong, Q.; Sum, T. C. Wavelength Tunable Single Nanowire Lasers Based on Surface Plasmon Polariton Enhanced Burstein-Moss Effect. *Nano Lett.* **2013**, 13, 5336-5343.

38. Liu, X.; Zhang, Q.; Xing, G.; Xiong, Q.; Sum, T. C. Size-Dependent Exciton Recombination

Dynamics in Single CdS Nanowires beyond the Quantum Confinement Regime. *The Journal of Physical Chemistry C* **2013**, 117, 10716-10722.

39. Citrin, D. S. Long radiative lifetimes of biexcitons in GaAs/Al<sub>x</sub>Ga<sub>1-x</sub>As quantum wells. *Physical Review B* **1994**, 50, 17655-17658.
40. Bacher, G.; Weigand, R.; Seufert, J.; Kulakovskii, V. D.; Gippius, N. A.; Forchel, A.; Leonardi, K.; Hommel, D. Biexciton versus Exciton Lifetime in a Single Semiconductor Quantum Dot. *Physical Review Letters* **1999**, 83, 4417-4420.
41. Liu, X. F.; Wang, R.; Jiang, Y. P.; Zhang, Q.; Shan, X. Y.; Qiu, X. H. Thermal conductivity measurement of individual CdS nanowires using microphotoluminescence spectroscopy. *Journal of Applied Physics* **2010**, 108.
42. Y. P. Varshni. *Physica (Amsterdam)* **1967**, 34, 149.
43. Honda, T.; Kawanishi, H.; Sakaguchi, T.; Koyama, F.; Iga, K. Characteristic temperature estimation for GaN-based lasers. *Mrs. Internet J. Nitride Semicond. Res.* **1999**, 4.
44. Ohtomo, A.; Tamura, K.; Kawasaki, M.; Makino, T.; Segawa, Y.; Tang, Z. K.; Wong, G. K. L.; Matsumoto, Y.; Koinuma, H. Room-temperature stimulated emission of excitons in ZnO/(Mg,Zn)O superlattices. *Applied Physics Letters* **2000**, 77, 2204-2206.
45. Wiersig, J. Hexagonal dielectric resonators and microcrystal lasers. *Physical Review A* **2003**, 67.
46. Gargas, D. J.; Moore, M. C.; Ni, A.; Chang, S.-W.; Zhang, Z.; Chuang, S.-L.; Yang, P. Whispering Gallery Mode Lasing from Zinc Oxide Hexagonal Nanodisks. *ACS Nano* **2010**, 4, 3270-3276.
47. Duan, X. F.; Huang, Y.; Agarwal, R.; Lieber, C. M. Single-nanowire electrically driven lasers. *Nature* **2003**, 421, 241-245.
48. Tang, Z. K.; Wong, G. K. L.; Yu, P.; Kawasaki, M.; Ohtomo, A.; Koinuma, H.; Segawa, Y. Room-temperature ultraviolet laser emission from self-assembled ZnO microcrystallite thin films. *Applied Physics Letters* **1998**, 72, 3270-3272.
49. Ushigome, R.; Fujita, M.; Sakai, A.; Baba, T.; Kubun, Y. K. GaInAsP microdisk injection laser with benzocyclobutene polymer cladding and its athermal effect. *Japanese Journal of Applied Physics Part I-Regular Papers Short Notes & Review Papers* **2002**, 41, 6364-6369.
50. Bhowmik, A. K. Polygonal optical cavities. *Appl. Optics* **2000**, 39, 3071-3075.
51. Liu, X.; Wu, B.; Zhang, Q.; Yip, J. N.; Yu, G.; Xiong, Q.; Mathews, N.; Sum, T. C. Elucidating the Localized Plasmonic Enhancement Effects from a Single Ag Nanowire in Organic Solar Cells. *ACS Nano* **2014**, 8, 10101-10110.
52. Ahmad, A.; Saq'an, S.; Lahlouh, B.; Hassan, M.; Alsaad, A.; El-Nasser, H. Ellipsometric characterization of PbI<sub>2</sub> thin film on glass. *Physica B: Condensed Matter* **2009**, 404, 1-6.

## FIGURES AND CAPTIONS

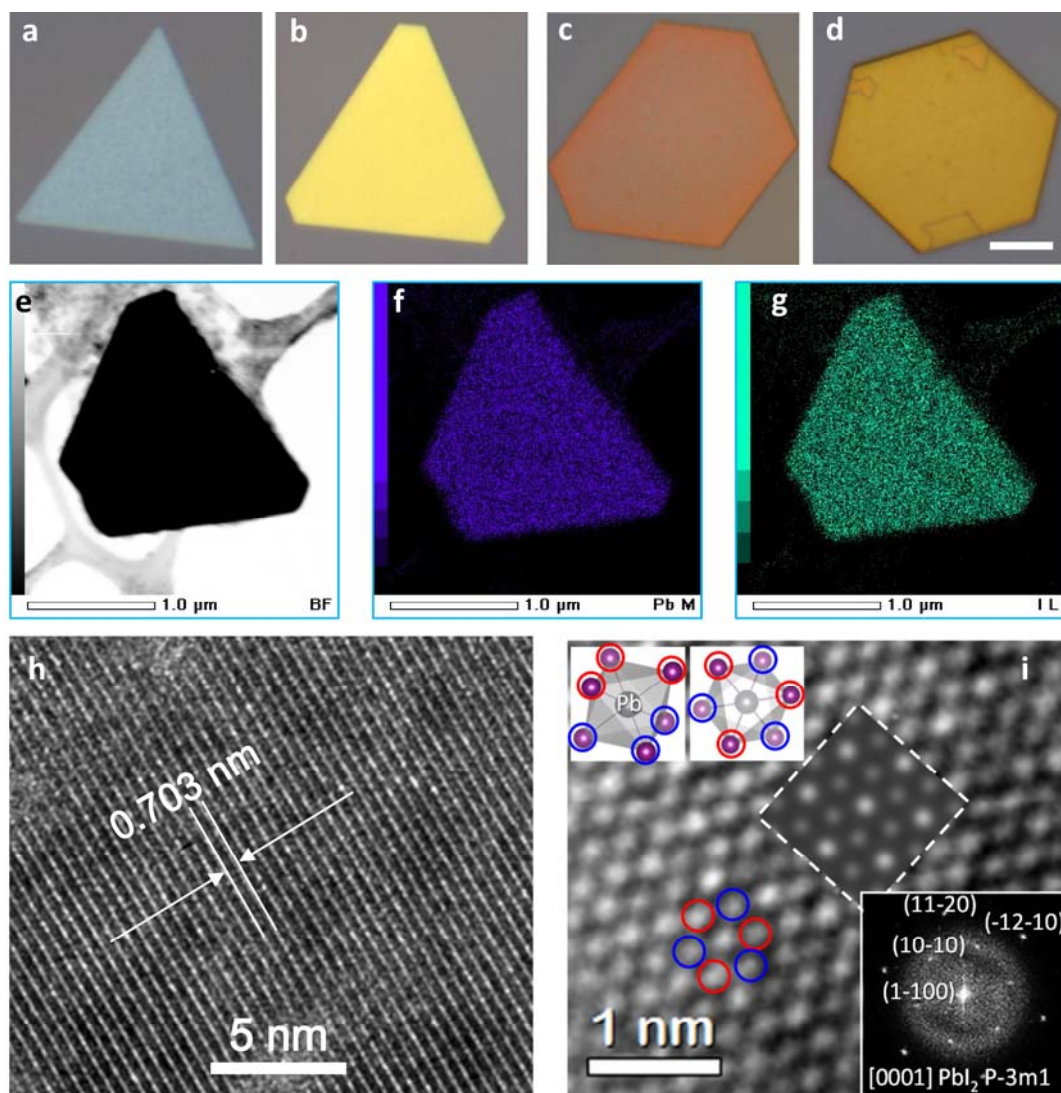


**Figure 1 Chemical-Vapor-Deposited PbI<sub>2</sub> platelets and characterization.** (a)-(d) Optical images of four representative PbI<sub>2</sub> platelets with different thickness of 40, 70, 105 and 500 nm. These platelets show planar, well-defined, polygonal structures. The angles between the polygonal edges are 30°, 60° or 120°, consistent with the atomic structures of PbI<sub>2</sub>. The scale bar is 5 μm. (e) Transmission electron microscope (TEM) image of a PbI<sub>2</sub> platelet. (f)-(g) The element mapping images obtained by energy-dispersive X-ray spectroscopy show the uniformity of the platelet of PbI<sub>2</sub>. (h) HRTEM structural analysis of the cross section of single-crystalline PbI<sub>2</sub> platelet, which shows a layer spacing of around 0.703 nm. (i) STEM-ADF image showing the hexagonal structure of the PbI<sub>2</sub>, red dashed circle (bright spot) is the top-layer iodine atom, blue dashed circle (dim spot) is the lower-layer iodine atom, the center position is the Pb atom. Top inset is a sketch of the PbI<sub>2</sub> structure from the top view, bottom inset is the Fast Fourier Transform pattern from the STEM-ADF image.

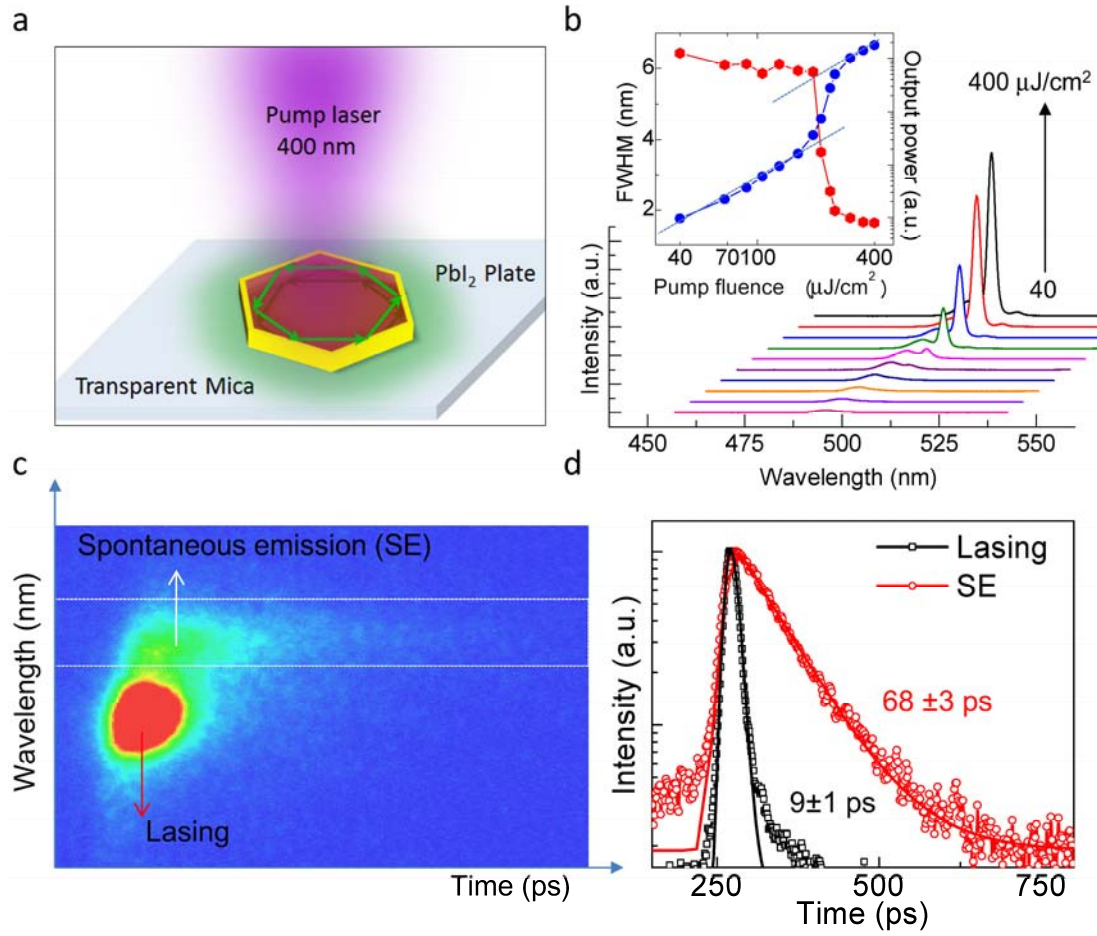


**Figure 2 Lasing Characterizations of whispering-gallery-mode hexagonal  $\text{PbI}_2$  platelet.** (a) Schematic representation of a single  $\text{PbI}_2$  platelet excited by a focused femtosecond pulse laser. (b) The evolution from spontaneous emission to lasing in a typical  $\text{PbI}_2$  hexagonal platelet, the pumping fluence increased from 40 to 400  $\mu\text{J}/\text{cm}^2$ . The inset shows power dependence of the integrated intensity and linewidth of the dominant emission feature, which gives a threshold of  $\sim 200 \mu\text{J}/\text{cm}^2$ . (c) A streak camera image of  $\text{PbI}_2$  platelet when the excitation fluence is above the threshold. (b) The decay profiles of the SE and lasing action are fitted using a mono-exponential decay function yielding lifetimes of  $68 \pm 3$  and  $9 \pm 1$  ps for SE and lasing, respectively.



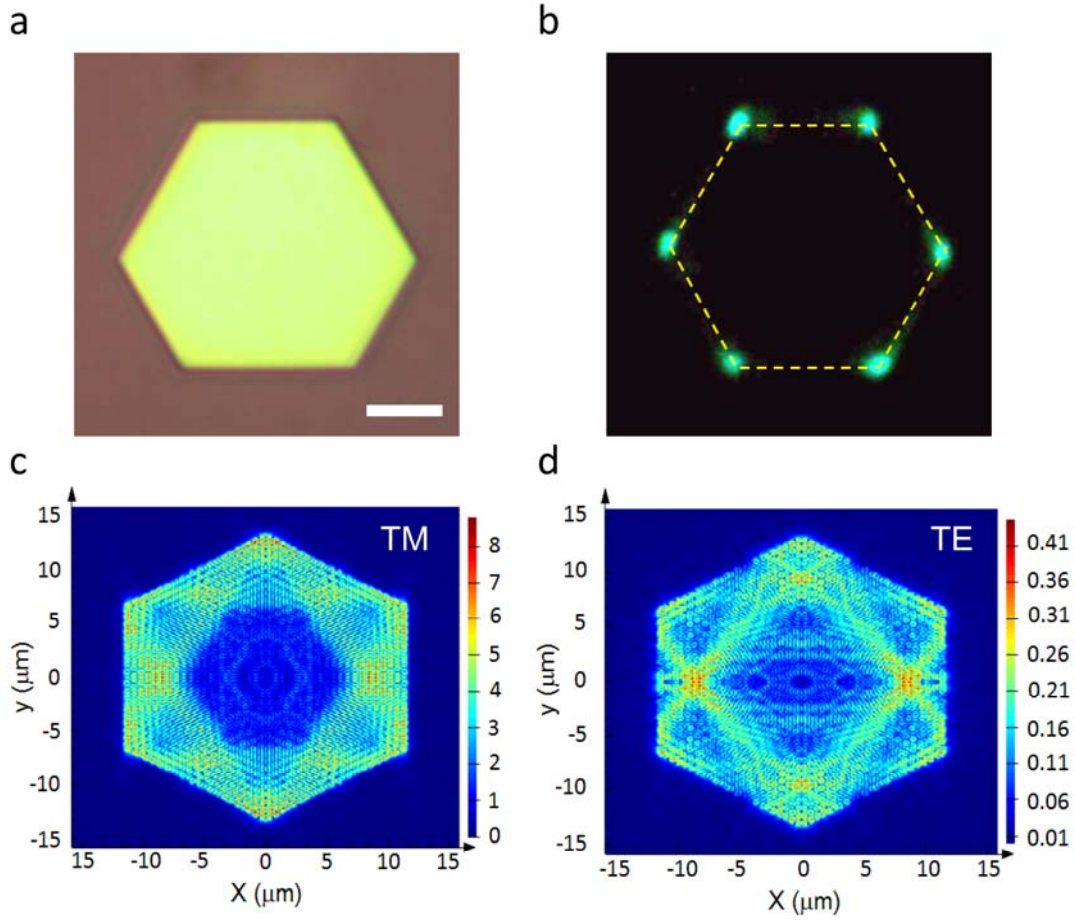


**Figure 3 FDTD simulation of the electric distribution inside the cavity for hexagonal  $\text{PbI}_2$  platelet.** (a) The optical image of a hexagonal platelet with thickness of  $\sim 150$  nm and edge length  $\sim 13$   $\mu\text{m}$ . The scale bar is 5  $\mu\text{m}$ . (b) The optical image in the CCD after filtering the pump laser line for a pump fluence of  $\sim 350$   $\mu\text{J}/\text{cm}^2$  (above threshold). (c)-(d) Simulated field distribution at resonant cavity mode of the typical hexagonal  $\text{PbI}_2$  platelets using TM (c) and TE mode (d).



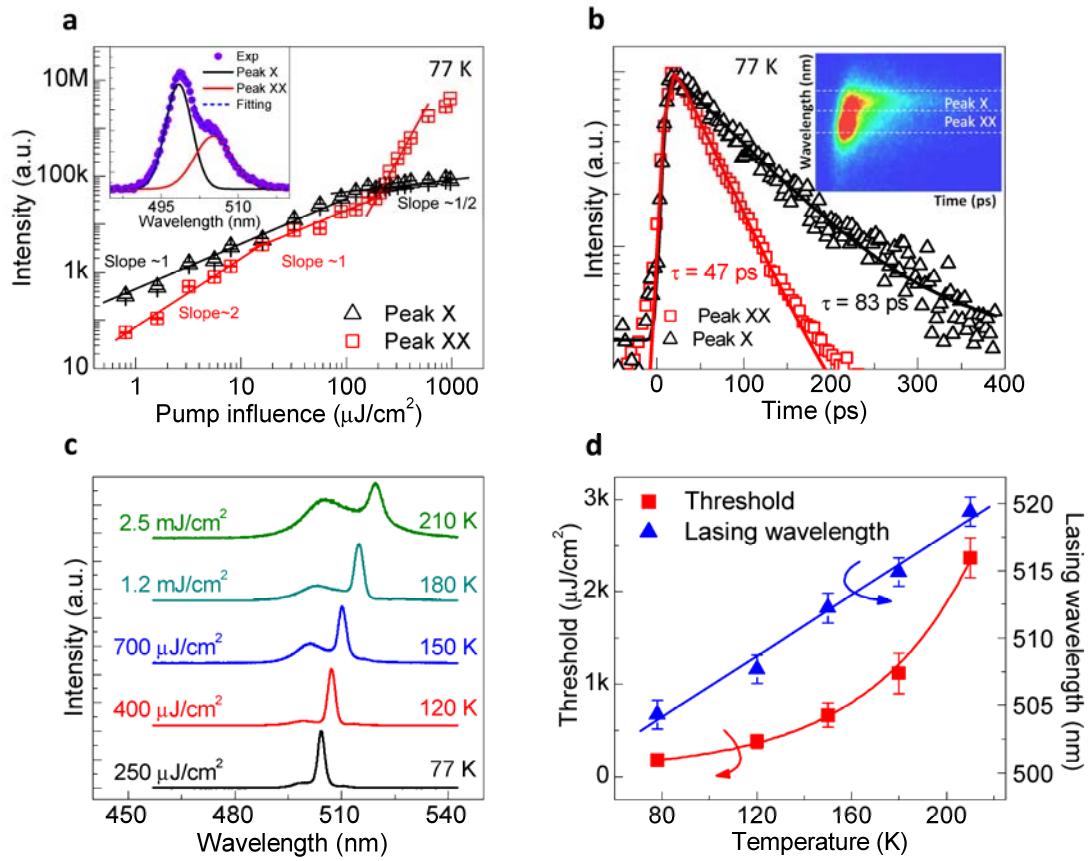


**Figure 4 Lasing mechanism and intrinsic properties of PbI<sub>2</sub> platelet.** (a) Excitation power dependent emission intensities of Peak X (open triangles) and Peak XX (open squares) in PbI<sub>2</sub> platelet at 77 K. Inset is the Gaussian fitting of PL spectra (at excitation fluence of ~40 μJ/cm<sup>2</sup>) of PbI<sub>2</sub>, the black fitting curve is band X and the red fitting line is band XX. (b) Time-resolved PL spectra of Peak X and XX and the inset is the corresponding time-energy two dimensional image of the PL emission. The pump fluence is fixed at ~40 μJ/cm<sup>2</sup> at 77 K. The decay profile of Peak X and XX are fitted with a mono-exponential function and the lifetimes are 83±3 ps and 47±2 ps, respectively. (c) The lasing spectra of a PbI<sub>2</sub> platelet at different temperatures (from 77 to 210 K). (d) Temperature dependent lasing threshold and lasing wavelength of PbI<sub>2</sub> are summarized. The blue line is the linear fitting and the red curve is the exponential function fitting result.

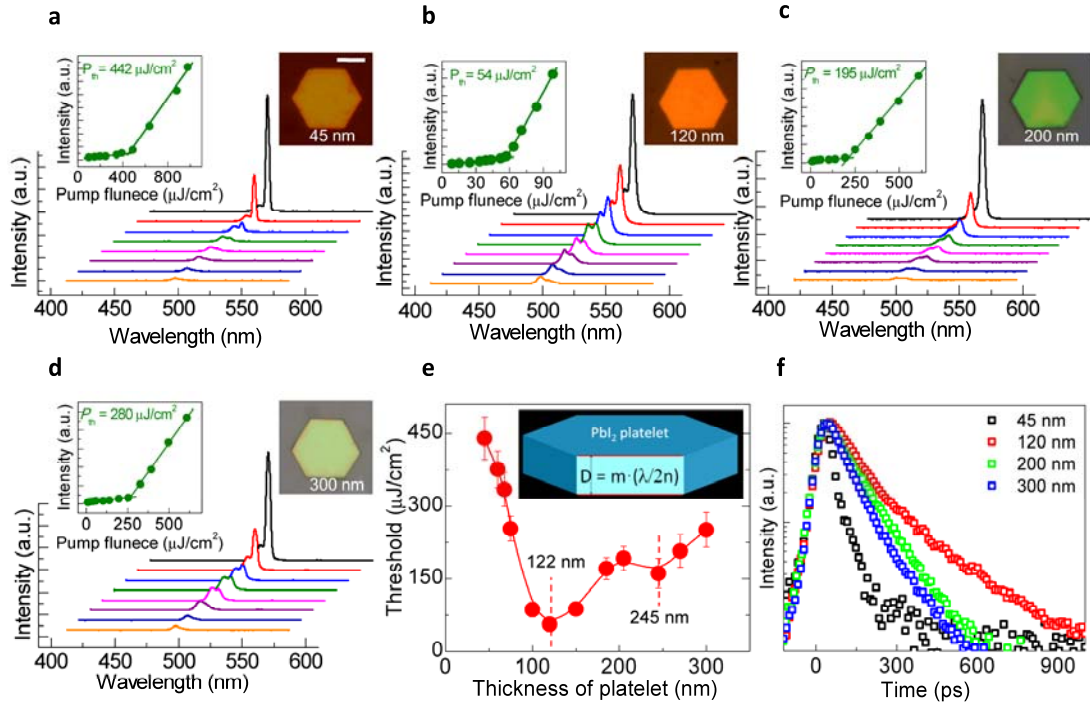


**Figure 5 Thickness dependent lasing thresholds in hexagonal  $\text{PbI}_2$  platelets.** (a)-(d)  $\text{PbI}_2$  hexagonal platelets emission spectra with increasing pump fluence from below threshold to above threshold, inset left is the plot of versus emission intensity, which shows the threshold of the sample, inset right is the optical image of the hexagonal platelet. The thickness of the platelet in a, b and c is  $\sim 45$ , 120, 200 and 300 nm, respectively. To reduce the influence of edge length of hexagonal platelet to the threshold of lasing, hexagonal platelets with nearly the same edge length are carefully selected for the study. The scale bar is  $10 \mu\text{m}$ . (e) Thickness dependent lasing threshold in a triangular  $\text{PbI}_2$  platelet, two dips or minima located at 122 nm and 245 nm are observed for low pump thresholds. (f) Decay profile of the biexciton peak (Peak XX) of the  $\text{PbI}_2$  hexagonal platelet with different thickness when excited at the same pump fluence of  $\sim 60 \mu\text{J}/\text{cm}^2$ .

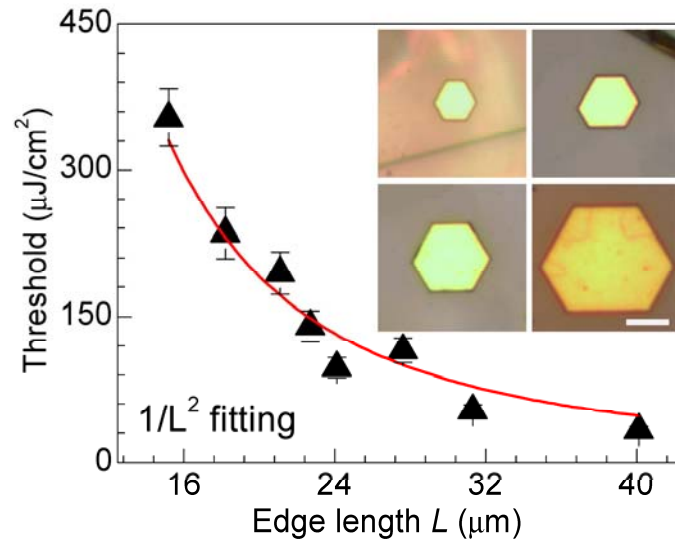


**Figure 6 Lasing thresholds versus edge length of the hexagonal PbI<sub>2</sub> platelets.** PbI<sub>2</sub> hexagonal platelets lasing thresholds (black triangles) are plotted as a function of edge length. The red curve is the fitting to a  $1/L^2$  trend. Inset are the optical images of a group of PbI<sub>2</sub> triangular platelets with different edge lengths but comparable thickness of  $200 \pm 20$  nm, the scale bar inside is 15  $\mu\text{m}$ .

## TOC GRAPHICS

